Basin-Scale Prediction of Sea Surface Temperature with Artificial Neural Networks

KALPESH PATIL AND M. C. DEO

Indian Institute of Technology, Bombay, Mumbai, India

(Manuscript received 2 January 2018, in final form 7 March 2018)

ABSTRACT

The prediction of sea surface temperature (SST) on the basis of artificial neural networks (ANNs) can be viewed as complementary to numerical SST predictions, and it has fairly sustained in the recent past. However, one of its limitations is that such ANNs are site specific and do not provide simultaneous spatial information similar to the numerical schemes. In this work we have addressed this issue by presenting basin-scale SST predictions based on the operation of a very large number of individual ANNs simultaneously. The study area belongs to the basin of the tropical Indian Ocean (TIO) having coordinates of 30°N–30°S, 30°–120°E. The network training and testing are done on the basis of HadISST data of the past 140 yr. Monthly SST anomalies are predicted at 3813 nodes in the basin and over nine time steps into the future with more than 20 million ANN models. The network testing indicated that the prediction skill of ANNs is attractive up to certain lead times depending on the subbasin. The ANN models performed well over both the western Indian Ocean (WIO) and eastern Indian Ocean (EIO) regions up to 5 and 4 months lead time, respectively, as judged by the error statistics of the correlation coefficient and the normalized root-mean-square error. The prediction skill of the ANN models for the TIO region is found to be better than the physics-based coupled atmosphere–ocean models. It is also observed that the ANNs are capable of providing an advanced warning of the Indian Ocean dipole as well as abnormal basin warming.

1. Introduction

a. SST and associated weather phenomena

The knowledge of sea surface temperature (SST) is fundamental to understanding the local and global climate variability. The changes in SST cause variations in the characteristics of weather phenomena, such as tropical monsoons and cyclones. The relationship between Indian Ocean SST and the Indian summer monsoon has been known for a long time (Shukla and Misra 1977). In particular, a high correlation among the warming of subbasins of the Indian Ocean (IO) and the amount and spatial spread of the annual rainfall in India has been well recognized (Yang and Lau 1998; Reddy and Salvekar 2003). The relative difference in SST across certain western and eastern subbasins gives rise to the events of the Indian Ocean dipole (IOD), which in turn leads to floods and droughts in the countries surround the tropical Indian Ocean (IO). The IOD is an important phenomenon occurring in the tropical Indian Ocean (TIO) and consists of alternate cooling and warming of the western IO (WIO) and eastern IO (EIO) in the late autumn months. If the heating of the WIO exceeds that of the EIO, then it becomes a positive IOD (pIOD) event and vice versa for a negative IOD (nIOD) event. (Saji et al. 1999; Saji and Yamagata 2003; Yamagata et al. 2004; Cai et al. 2014). The prediction of SST a few months in advance also enables the prediction of rainfall across the Indian subcontinent (England et al. 2009; Sahai et al. 2003; Ummenhofer et al. 2009; Reddy and Salvekar 2003). It is reported that the IO, especially the WIO, has a higher warming trend than other oceans (Roxy et al. 2014), and this leads to more frequent IOD events and the resulting flood and draft situations (Rao et al. 2012; Roxy et al. 2014).

SST plays a significant role in tropical cyclone (TC) genesis. The impact of a TC can be evaluated by the power dissipative index (PDI), which is an integral of the cube of maximum sustained wind speed in a storm (Emanuel 2005). The TCs occurring in the northern IO are found to be in good agreement with the PDI, especially during the premonsoon season (Sebastian and Behera 2015). It is also observed that the IO SST strongly controls the TCs occurring in the Pacific region (Zhan et al. 2014), the Australian basin (Saha and Wasimi

Corresponding author: M. C. Deo, mcdeo@civil.iitb.ac.in

DOI: 10.1175/JTECH-D-17-0217.1

2013), the South China Sea (Wang et al. 2013), and Korean waters (Choi et al. 2015). SST not only aids in TC genesis but can intensify a TC and change its path (Michaels et al. 2006; Yu and McPhaden 2011). As per Magee et al. (2015), a TC occurring over the Pacific region can shift toward the east or west as per the heating or cooling of EIO SST anomalies.

The SST has a strong influence on marine biodiversity, and the knowledge of potential changes in the SST is helpful in locating likely fishing zones (Solanki et al. 2015; Lee et al. 2005). In the Arabian Sea (AS) and Madagascar regions, productivity of the yellowfin tuna is stated to be lower during the positive IOD and vice versa (Lan et al. 2013). The coral reefs, of great importance in the marine ecosystem, show lower growth rate in the western and central IO as a result of their intense warming (Roxy et al. 2014; Abram et al. 2003). The reefs of the Mentawai Islands were tragically harmed in 1997 as a result of a strong positive IOD that also led to one of the worst wildfires in Southeast Asia (Abram et al. 2003).

b. *SST predictions*

The SST provides vital input to coupled ocean–atmosphere general circulation models (COAGCMs) in the form of boundary conditions. Such models require regularly predicted SST fields for model integration. Accurate SST predictions can help in understanding rainfall patterns a few months earlier and also can assist in tracking the cyclone genesis and in planning the marine ecosystem. In the past SST predictions have been reported by many researchers using complex physics-based models, statistical methods, and nonlinear forecasting techniques. The physics-based models include COAGCMs (Saha et al. 2014; Stockdale et al. 2011; Luo et al. 2005; Francis et al. 2013) and Modular Ocean Models (MOMs) (Saha et al. 2006; Alves et al. 2003; Wang et al. 2011; Thompson et al. 2005). They involve a large number of assumptions and also require large exogenous data (Francis et al. 2013) for model start up and time integration. The performance of physics-based models depends on the data assimilation schemes and coupling mechanisms used, and further: these models predict many parameters at the same time, making accurate tuning for a single parameter of interest a difficult task.

The statistical techniques of SST prediction include linear regression (Kug et al. 2004; Tang et al. 2000; Tripathi et al. 2006), Markov models (Xue and Leetmaa 2000), analog techniques (Agarwal et al. 2001), canonical correlation analysis (Collins et al. 2004; Tang et al. 2000), and forced red noise process (Jansen et al. 2009). Gupta and Malmgren (2009) considered several statistical methods and concluded that the SST predictions made by all were associated with high values of root-mean-square (rms) errors. The prediction of leading principle components or empirical orthogonal functions of SST is an additional and alternate approach (Álvarez 2003; Álvarez et al. 2004; Wu et al. 2006; Neetu et al. 2011; Tang et al. 2000; Collins et al. 2004).

As an alternative to these traditional methods in the form of artificial neural networks (ANNs), genetic algorithms and support vector regressions have therefore been adopted. Tripathi et al. (2006) indicated the usefulness of ANN-based SST predictions for monthly scales. Garcia-Gorriz and Garcia-Sanchez (2007) attempted prediction of SST using ANN and found that the ANN, apart from providing good accuracy, also captured an important climatic event of a heat wave in the summer of year 2003. Aguilar-Martinez and Hsieh (2009) explored many nonlinear methods for SST predictions and found the ANN to be more effective than other nonlinear methods from both a modeling and prediction skill perspective. Mahongo and Deo (2013) investigated the skill of SST prediction by ANN on monthly and seasonal scales and found that ANN is attractive for up to a few time steps into the future. Patil et al. (2016) explored the use of combined numerical and neural techniques for updating the SST predictions and showed that such combined models performed better than the numerical-only methods. In an another study, Patil and Deo (2017) demonstrated the usefulness of certain wavelet neural networks in daily SST predictions.

c. *Objective and scope*

There are many advantages of ANN over traditional statistical or numerical methods. Basically, ANNs are model-free estimators in that no fixed mathematical form is assumed a priori in between the input and output. They are data oriented rather than model oriented and learn by examples instead of hard definitions; thus, they can be viewed as close to the real world. Although the use of ANN has been found to be very attractive in many recent studies, it suffers from the limitation of being site specific in nature. In this work we have tried to address this by developing SST prediction models applicable for large spatial domains. Such large domain predictions should help in truly understanding its competence with physics-based models. We have primarily focused on monthly SST predictions in the IO region over a time horizon of nine months in advance. We have compared our ANN predictions with leading COAGCMs and MOMs, and assessed the potential of ANNs in capturing weather phenomena of extreme IOD and unusual basin warming. The ANN-based real-time prediction of IOD events is an additional feature of this study.

This paper is structured as follows. Section 2 describes the reanalysis data used in the training of ANN models. Section 3 gives details of the ANN modeling, while section 4 discusses the prediction skill and the seasonal dependency of the SST anomaly (SSTA) over the TIO region. Section 5 presents validations of SSTA predictions with respect to some important oceanic events, including IOD and basin warming. An attempt to predict real-time IOD with the help of ANN is described in section 6, which is followed by a discussion summary in section 7.

2. Data

The Hadley Centre Sea Ice and SST dataset (HadISST) is used in this study. HadISST is reconstructed from various datasets by a two-stage reduced-space optimal interpolation method. The sets of data include the Met Office Marine Data Bank (MDB), the International Comprehensive Ocean–Atmosphere Data Set (ICOADS), the Global Telecommunication System (GTS,) and the Advanced Very High Resolution Radiometer (AVHRR) SST. To improve the quality of data and to capture various climate and oceanic signals, gridded observations were superimposed onto reconstructed datasets. Being a blend of diverse SST products, HadISST is however prone to bias, which was adjusted by smoothening with appropriate filters for gridded observations and by using in situ observations. The bias adjustment has produced a uniform variance over the time scale. Additional details in this regard can be found in Rayner et al. (2003). The HadISST data have replaced earlier Global Sea Ice and SST datasets (GISST), and they are in the form of monthly SST fields with 1° spatial resolution and run through January 1870 to the present. The data are updated on the 10th day of every month and are available for one month prior to the latest month. In this study we have used data from January 1870 to August 2017 (147 yr and 8 months), incorporating a total of 1772 observations at each grid.

Although other types of monthly SST datasets were available—for example, Extended Reconstructed SST (ERSST), Centennial In Situ Observation-Based Estimates (COBE), Lamont-Doherty Earth Observatory (LDEO), and Kaplan SST—they have either coarser spatial resolution or do not have regular time updates. A coarse resolution may not capture significant oceanic and climate signals, while irregular time updates are more suitable for the purpose of analysis rather than forecasting (Yasunaka and Hanawa 2011).

3. ANN modeling details

In this study we have used the feed-forward back-propagation (FFBP) architecture of ANN for predicting future values of monthly SSTA. Although alternative architectures are available in the form of radial basis functions, generalized regression neural network, and wavelet neural network, FFBP was preferred in view of its simple configuration and fast processing speed appropriate for the present problem. A review of ANN applications in ocean science and engineering by Jain and Deo (2006) and Deo (2010) indicated that the use of FFBP is common and also adequate for many applications, although hybrid networks like the wavelet neural network can also be of benefit (Patil and Deo 2017). The SSTA data were formed by subtracting the long-term mean from absolute SST values. The use of anomalies in place of absolute values enabled a more appropriate comparison of the predicted versus target SST. The ANN had three layers, namely, input, hidden, and output, in which the input layer consisted of neurons representing the sequence of past SST values. To determine the most appropriate number of past SST values, 60 different combinations were experimented. Examples of these combinations are given in the appendix. The number of neurons in the hidden layer was set by trials, aimed at getting the best performance in training as judged by the error statistics mentioned subsequently. The number of neurons in the output layer was 1 and this belonged to the predicted value. Although many alternative transfer functions are available to train an ANN, we have used the *tan-sigmoid* transfer function in the hidden layer and *linear* in the output layer as done in many other studies (Jain and Deo 2006). The training samples were divided into subsets of training, cross validation, and testing in proportions of 75%, 5%, and 20%, respectively.

The SST data belonging to the TIO region were extracted from the global HadISST information. The SST values here are specified at each node of 1° × 1° rectangular grids. The total number of nodes was 3813. At each node the absolute SST was converted into its anomaly values by subtracting the long-term mean of 30 yr varying from 1961 to 1990. A separate ANN model was set up to predict the SSTA for a given lead time and such lead times (months) were nine in total. Thus, there were 3813 × 9 ANNs. Each ANN model was trained with 60 sets of input combinations (see the appendix). During training and for every input combination, 10 different random initial conditions (numbers) were used to reduce the effect of initial conditions. The optimization algorithm of Levenberg–Marquardt (LM) was used for training, as it has the advantage of providing fast and efficient training (Marquardt 1963; Hagan and Menhaj 1994). The training aim was to minimize the mean squared error between the realized and the target output. The resulting best model out of those corresponding to 10 different initial conditions and 60 different input combinations was retained. Thus, a total of 3813 × 9 best

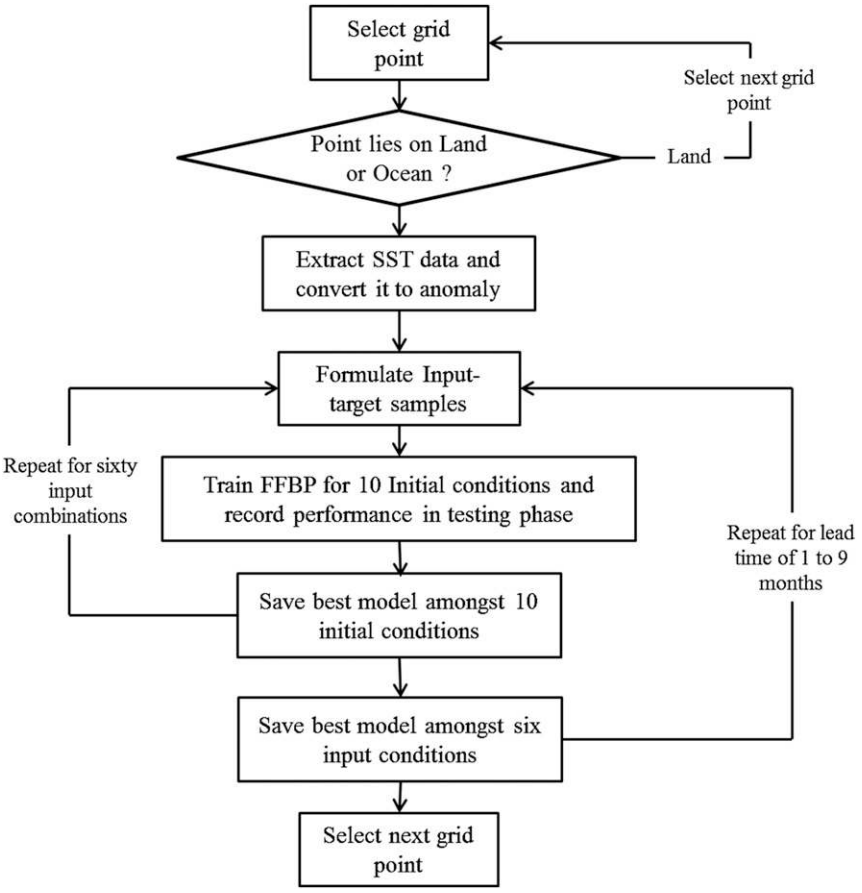

FIG. 1. Flowchart for modeling monthly SSTA using ANN.

models were retained out of 20.5902 million ANNs, resulting from 3813 nodes, nine lead months, 60 input combinations, and 10 initial conditions. These details in the form of a flowchart can be seen in Fig. 1. The details of ANN functioning along with those of the training process can be seen in Anderson (1995).

4. Prediction skill of SSTA in TIO

This section describes the prediction skill of SSTA in the TIO during the testing phase of 27 years, ranging from January 1990 to December 2016, in terms of the error statistics of the correlation coefficient (r), normalized root-mean-square error (NRMSE). Figure 2 shows the spatial variation of r between the observed and predicted SSTA when the lead time changed from 1 to 9 months. It can be seen that the prediction skill ($r > 0.5$) is good up to 3 months in most parts of the TIO and becomes worse after 5 months. This performance is improved compared with the predictions based on the numerical CFSv2 model, in which case the skill was found to worsen after 3 months by Zhu et al. (2015). Figure 2 indicates that with the increasing prediction horizon, the SSTA predictions in the AS region remain attractive until 3 months versus 5 months in the Bay of Bengal (BoB) region. The EIO region is associated with poorer skill than the other TIO regions. An accurate prediction even up to 6 months into the future can be seen in the WIO region unlike other regions of the TIO. The southwestern part of the TIO, eastward from Madagascar, belongs to the highest prediction skill among the other regions of the TIO with $r > 0.4$ even at 9 months lead time. We find that compared to the persistence model–based predictions in Zhu et al. (2015), our ANN-predicted SSTA is much better even up to 5 months lead time compared to their 2-months-ahead predictions for which the r value exceeded 0.4, with the exception of the WIO region.

The WIO and EIO subbasins have importance in the formation of IOD. Hence, the model skill in these regions was further analyzed. Figure 3 shows the average prediction skills in WIO and EIO. In the WIO region, r is more than 0.6 up to 4 months lead and falls thereafter, but it remains above 0.4 until 9 months. A similar observation can be made for the EIO region, except that

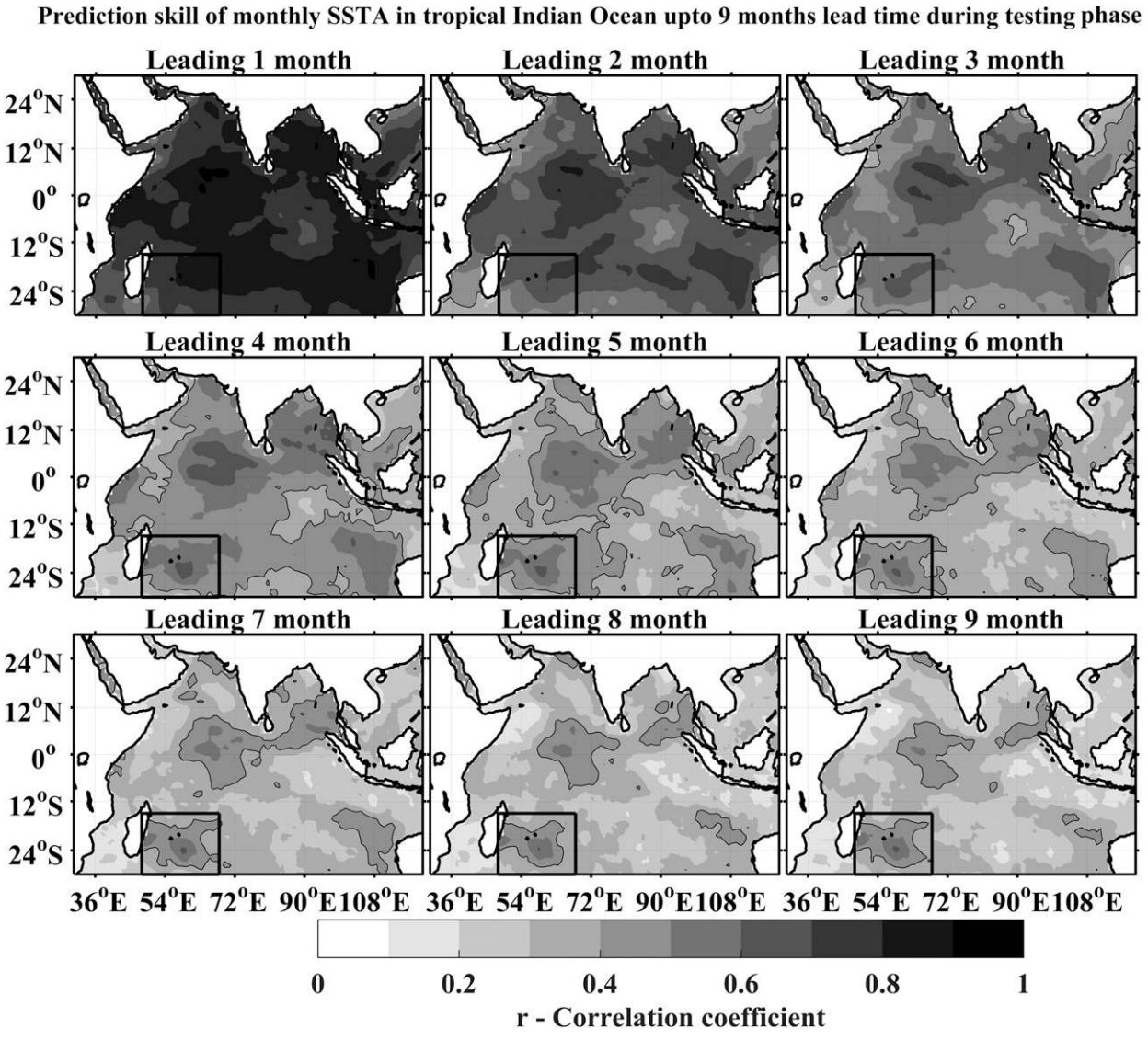

FIG. 2. Spatial variation of the coefficient of correlation between observed and predicted SSTAs using ANN over TIO as a function of lead time from (top left) 1 to (bottom right) 9 months. The rectangle shows the region with the best performance, especially at higher lead times.

here the skill starts decreasing after 3 months. We have noted that this prediction skill is better than a few coupled physics-based models, such as SINTEX-F, CFSv1, the Predictive Ocean Atmosphere Model for Australia [POAMA 15b (P15b)], and the ECMWF Seasonal Forecast System 3 (ECSys3) (Shi et al. 2012).

The statistic NRMSE is a ratio of RMSE to the standard deviation of observed data; hence, when predictions have the standard deviation exceeding that of the observations, the limit of predictability is supposed to have been reached. For both regions NRMSE is below 1.0 up to the 9 months lead time, but the EIO has a higher NRMSE than the WIO. This difference can be due to the variations in the SSTA of both regions in that the WIO has higher persistence than the EIO. For both regions the average limit of predictability is up to 9 months, but the EIO reached it faster than the WIO.

For assessing the long-range predictability, seasonal prediction skills were further analyzed. Figure 4 shows the same for both the western and eastern regions in the IO responsible for generating IOD episodes. It is seen that the WIO had better predictability in autumn than in spring. In autumn r is more than 0.6 even at 6-months-ahead prediction in the WIO region, whereas in spring r is limited to 3 months. The opposite seems to be true for the EIO region, where the spring season corresponded to a better skill ($r > 0.6$) up to 7 months lead time than the 2 months lead time of the autumn season. Thus, the IOD prediction is better in spring than in autumn.

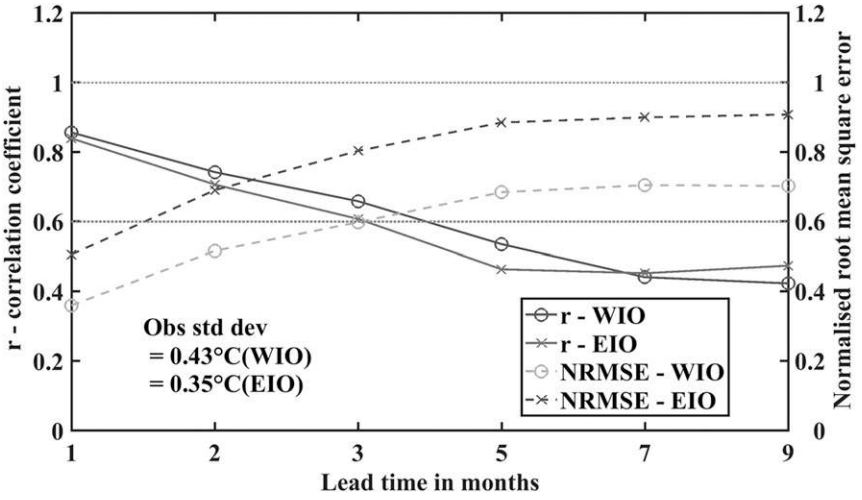

FIG. 3. Variation of *r* and NRMSE with lead time averaged over WIO and EIO regions.

Although IOD usually occurs in September–November, the prediction was good only up to a lead time of 2 months, unlike the case of early spring months. Despite that March and October are both warmer months, the ANN performance in March was better for both the WIO and EIO regions ($r > 0.6$; lead time: 3–6 months), whereas in October it was better only for the WIO region ($r > 0$ 0.6; lead time: 6 months) and it deteriorated in the EIO region ($r > 0.6$; lead time: 2 months). This clearly indicates that the accuracy of IOD prediction largely depends on the prediction skill in the EIO region, especially in autumn.

5. Event-based validation

In the preceding sections, we presented different prediction skills of the SSTA over the TIO region.

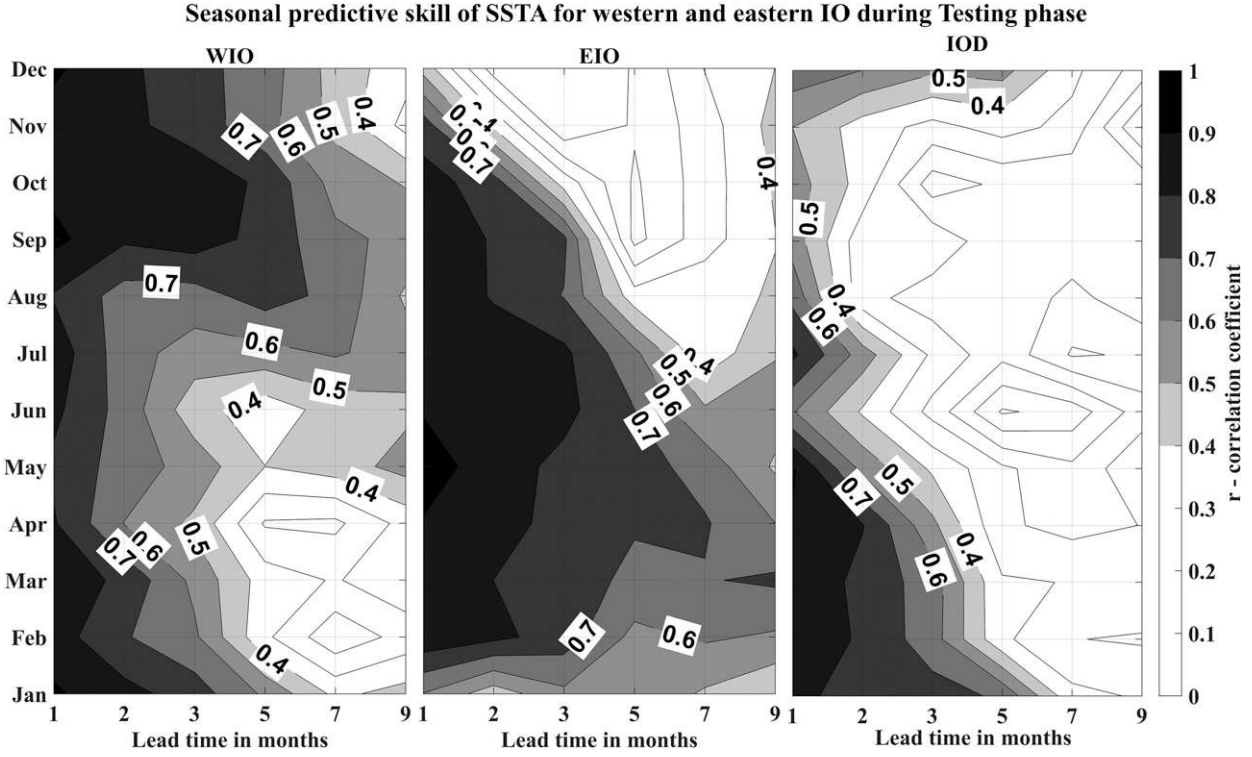

FIG. 4. Variation of *r* with lead times (months) from December to January during SSTA predictions over (left to right) the WIO, EIO regions, and IOD index.

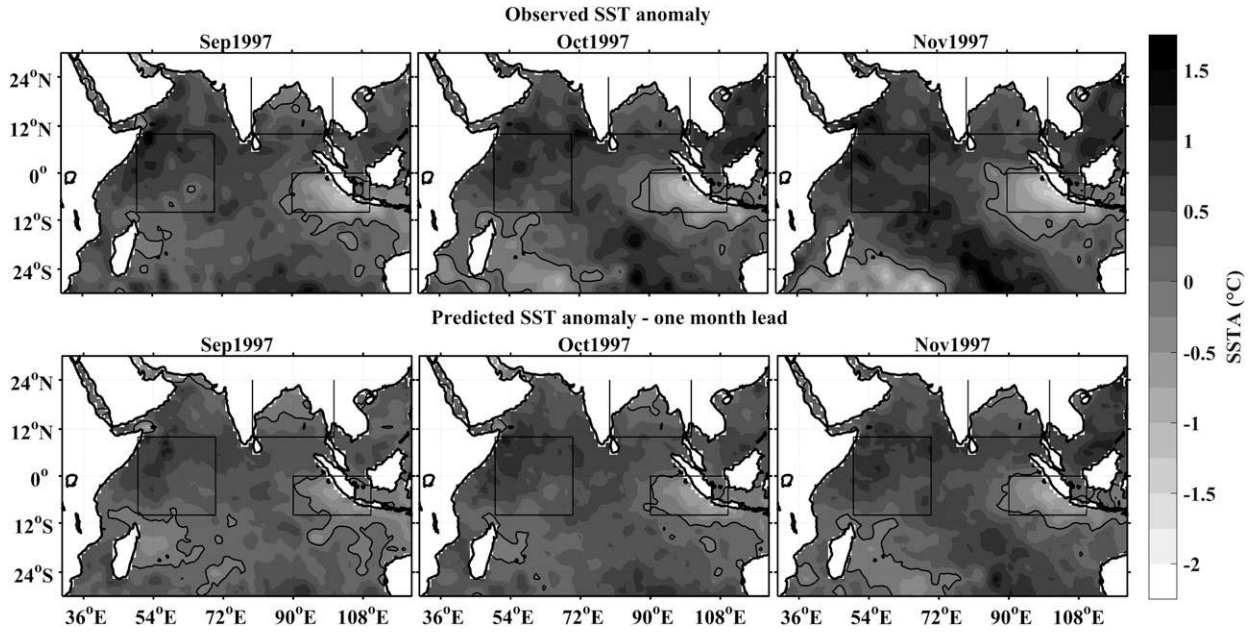

FIG. 5. (top) Observed SSTA vs (bottom) ANN-predicted SSTA for a 1-month lead time during (left to right) September, October, and November of the extreme pIOD of 1997. Within each panel, the left square and right rectangles focus on the WIO and EIO regions, respectively; the upper square with the open top focuses on an unusual warming in the BoB region. The thick black contour is the 0°C SSTA.

However, this pertained to an overall or average ANN performance. We subsequently checked the ability of the trained ANN in capturing the events of extreme IOD and basinwide warming. This is discussed below.

a. IOD events

We have analyzed the ANN predictions at the time of two extreme pIOD events, in 1997 and 1994, and one nIOD event, 1996 (Webster et al. 1999; Yamagata et al. 2004).

1) 1997 PIOD EVENT

The pIOD that happened in the year 1997 was very strong and in this event not only the SSTA in the WIO was more than that in the EIO but both regions had SSTA exceeding 1.5°C. This strong IOD had profoundly impacted the local climate. The worst wildfires of Southeast Asia, the destruction of coral reefs on the Mentawai Islands in late 1997, and the damage to the ecosystem in various parts of the TIO (WIO, central IO, Sumatra, and Indonesia) have been attributed to it (Abram et al. 2003). Figure 5 shows the observed SSTA during September–November and their comparison with 1-month-ahead predictions of SSTA.

It may be seen that the predicted SSTA had captured the warm and cold fronts (0°C contour) well. Apart from this a warm band starting from the AS, extending to the central part from the WIO, and ending in the southeastern part was also fairly predicted fairly. A warm (cold) bias is seen in the WIO and EIO. The EIO has a higher bias compared to the WIO. Further, the BoB region was supposed to be cool during pIOD, but in 1997 it became unusually warm. Such unusual warming of the BoB was also fairly represented in the ANN predictions.

2) 1994 PIOD EVENT

Another extreme pIOD was observed in 1994 in which both the WIO and EIO regions exceeded SSTA beyond +1° and −1°C, respectively. This event caused an unusually hot and dry summer in East Asia (Kawamura et al. 1998; Guan and Yamagata 2003). Figure 6 shows a comparison of a 1-month-ahead prediction and observation for the 1994 pIOD.

A similar nature in predictions (as in the 1997 pIOD) resulted in the pIOD of 1994. Moreover, this 1994 pIOD has shown better predictability than the earlier 1997 pIOD, if we look at the 0°C contour. In case of the 1994 pIOD, the SSTA predictions of November were better than those of September and October.

3) 1996 NIOD EVENT

To understand the difference between the pIOD and nIOD cases, we have considered the nIOD that occurred in 1996. Figure 7 shows the observed nIOD versus corresponding 1-month-ahead predictions. In 1996 nIOD some part of the WIO at the 0°C contour was not represented properly. Except for this, both the warm and cold regions were well simulated in the nIOD.

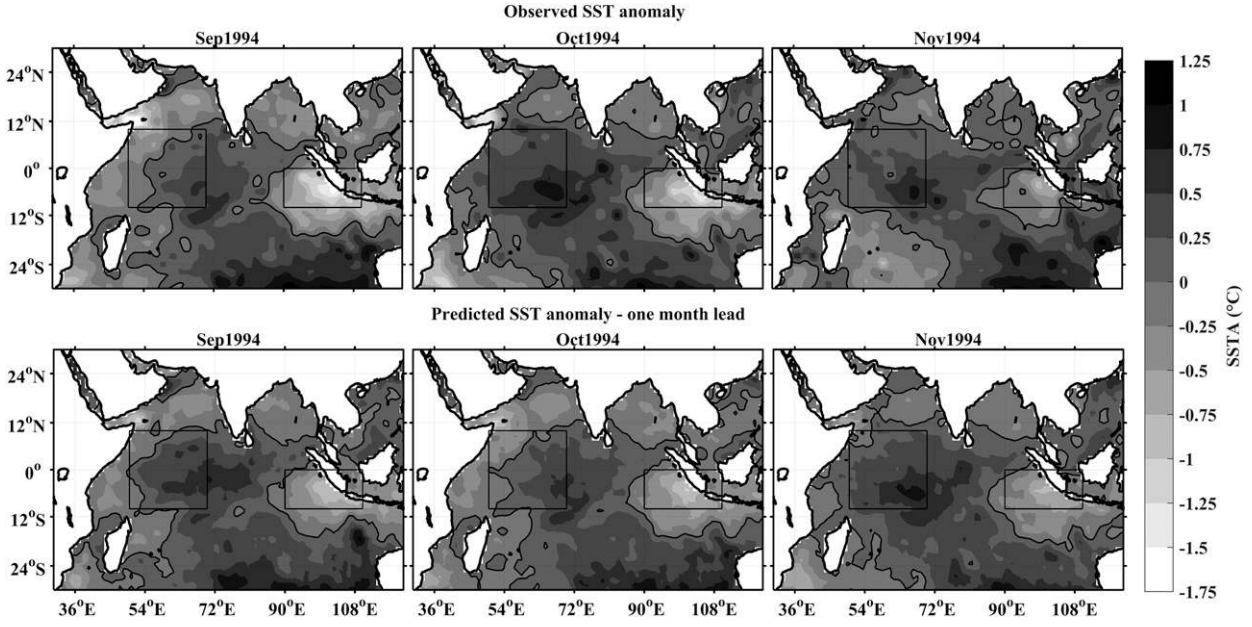

FIG. 6. As in Fig. 5 but during the extreme pIOD of 1994 (and without the upper square).

In both the pIOD and nIOD predictions, bias was observed in both colder and warmer regions, but their separation boundaries were well followed, unlike the case with the Modular Ocean Model as in Thompson et al. (2005), where intrusion of the colder region in the WIO (or EIO) for pIOD (or nIOD) was observed along with a higher bias than the ANN predictions. Comparing the pIOD and nIOD predictions, the pIOD had shown more bias than the nIOD. Also, the ANN prediction of the relatively milder event of the 1994 pIOD was more accurate than that of the 1997 pIOD.

b. *Abnormal basinwide warming in TIO*

The TIO basin was observed to be abnormally warm during years 2000 and 2008. This warming had severely affected the Indian summer monsoon in which the

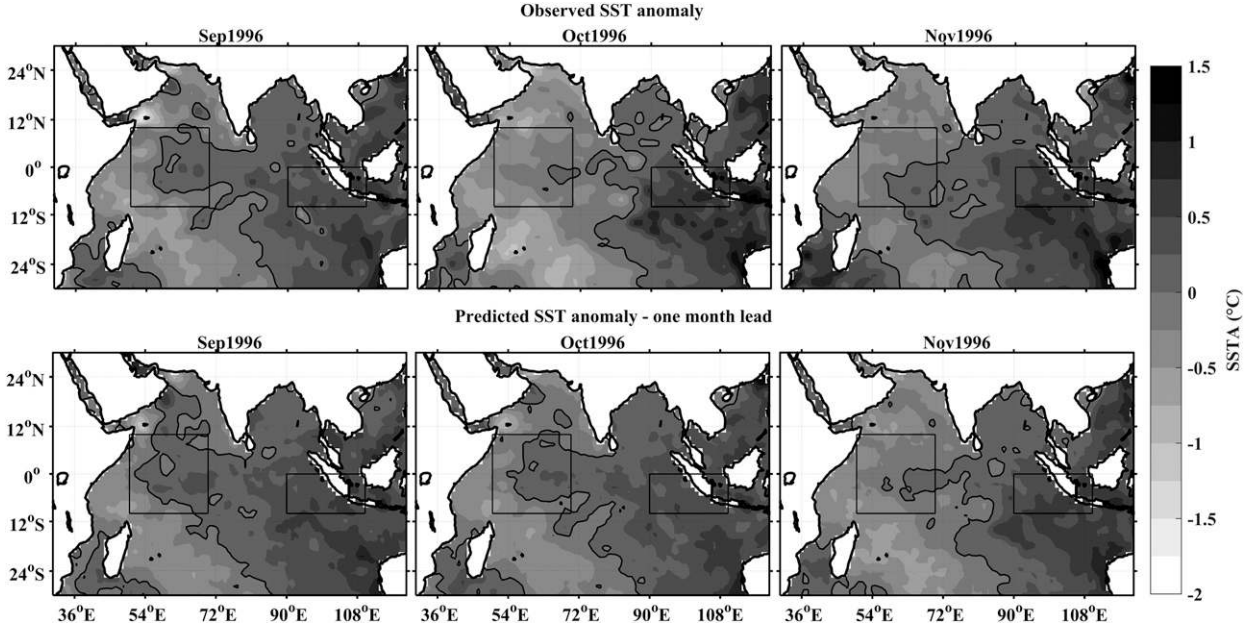

FIG. 7. As in Fig. 6 but during the extreme nIOD of 1996.

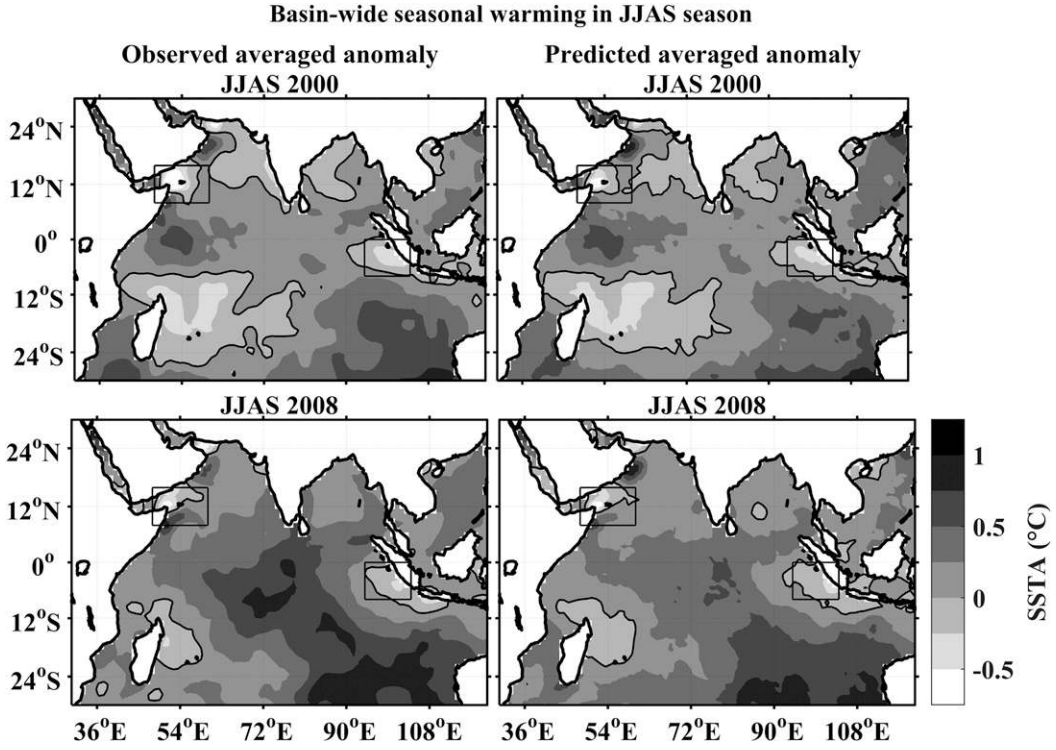

FIG. 8. Seasonally averaged (left) SSTA observations vs (right) predicted SSTA for a 1-month lead in JAS in (top) 2000 and (bottom) 2008 over the TIO. Within each panel the left (right) rectangle highlights the northern Somali (west coast of Sumatra) region.

Indian subcontinent experienced a suppressed rainfall, especially in the central part of India, and enhanced rainfall over the equatorial and southern tropical IO (Krishnan et al. 2003; Rao et al. 2010). Figure 8 shows the averaged SSTA during June–September (JJAS) of 2000 and 2008 over the TIO and its comparison with predicted JJAS SSTA.

In the year 2000, tropical and southeastern parts were warmer than other parts and the southeastern one was the warmest with the SSTA moving up to 0.75°C. A normal cooling was observed in the AS, the BoB, the EIO, and the southwestern part of the TIO. Another thing to notice was a very cold spot (approximately less than −0.75°C) in the western AS above the Somali coast. Predictions in JJAS of 2000 simulated the 0°C SSTA contour well in the TIO. Colder regions (0° to −0.5°C) of the southeastern part of the AS and BoB were also captured very well. Also, the cold spot of the western AS and a small part in the EIO near the coast of Sumatra were well located along with matching of the magnitudes. Only the southeastern warming was somewhat underestimated in the predictions.

The colder regions of 2008 were smaller than those of 2000, and the warming of the tropical and southeastern parts was enhanced. This enhanced warming was more than 1°C. In 2008, these colder regions were well captured like in the year 2000. Similarly, the warmer zones of tropical and southeastern parts have shown underestimation. In general, the basinwide warming of 2000 was better modeled than that of 2008.

c. *Abrupt Red Sea warming*

It is known that the Indian Ocean is undergoing continuous warming with the changing climate (Rao et al. 2012; Cheng et al. 2017). Such warming was also noticed in the Red Sea. The Red Sea has a rich marine ecosystem with a high amount of biodiversity and coral reefs. Because of the warming of the Red Sea, the growth of coral reefs and other marine life has slowed down by 30% in the recent past (Cantin et al. 2010). Such warming on the order of 0.7°C is experienced after the year 1994 (Raitsos et al. 2011).

In Fig. 9 progression of the warming is shown from 1990 to 2016 for the two cases: observed and modeled. In early 1990 the sea region was cooler, but from 1994 it started warming and continued with 2010 as the warmest year during which the SSTA was more than 1°C throughout the year. The right column of Fig. 9 shows the ANN-based SSTA predictions, which also depicts a similar progression pattern of warming from 1990 to 2016. The peak year of 2010 was also noticed clearly in these predictions. The annual average SSTA (observed

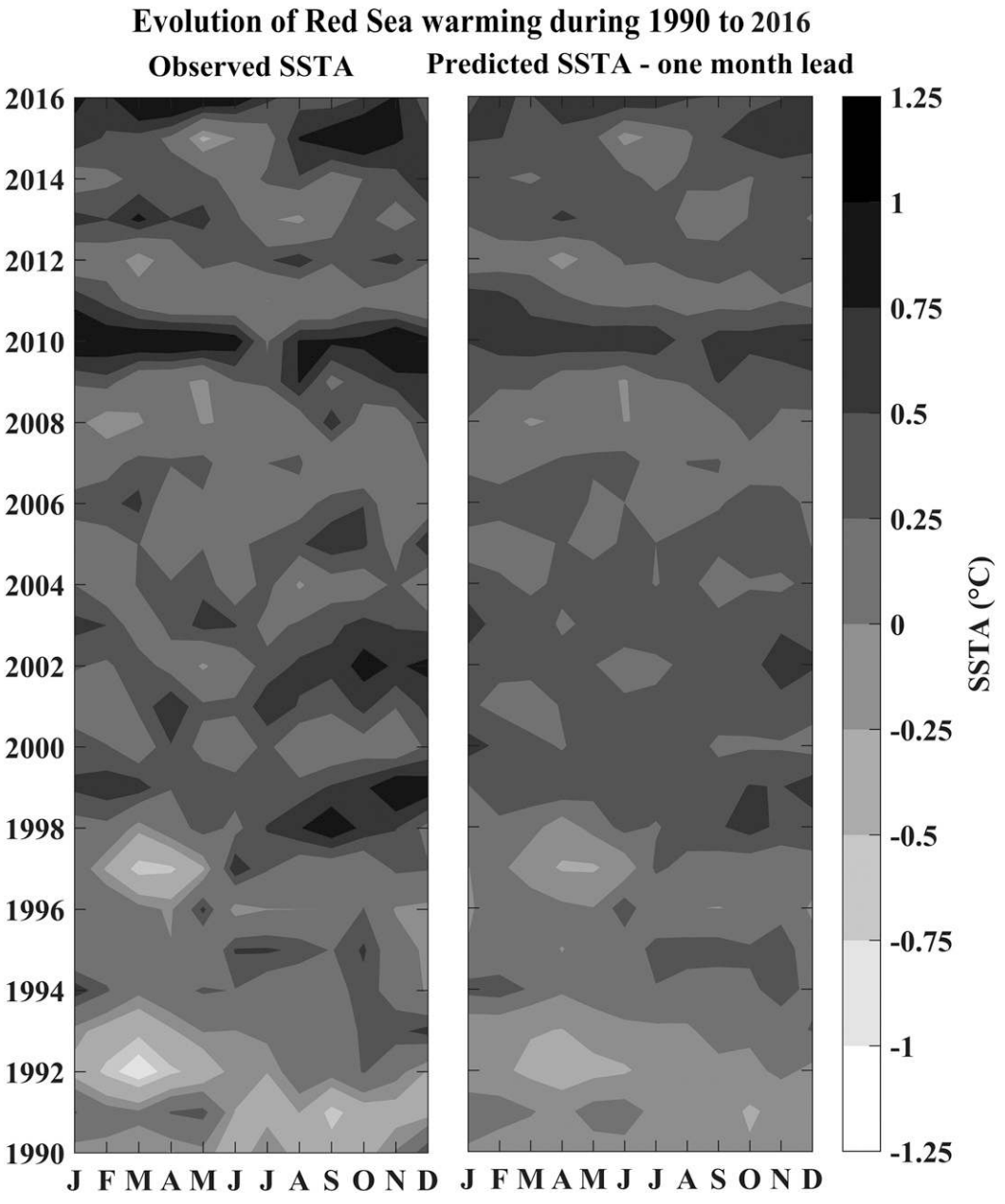

FIG. 9. Evolution of the intraseasonal warming over the Red Sea from 1990 to 2016. (left) Spatial average of observed SSTA. (right) As in the left panel, but for the predicted SSTA for a 1-month lead time.

as well as predicted) during this peak warming year of 2010 is shown separately in Fig. 10. Most of the warming occurred in the northern part of the Red Sea.

6. Real-time prediction of IOD

We have also attempted a real-time forecast of the IOD events. As the HadISST data are updated at every 10th day of the preceding month, a complete SSTA for the past month from the given current month was not available. To fill this gap we used the National Oceanic and Atmospheric Administration (NOAA), version 2 (v2), reanalysis dataset on the monthly scale. These data also consist of an amalgamation of various datasets, optimally interpolated to spatial grids of $1° \times 1°$.

Apart from filling the gap, the NOAA data were also used to carry out a correlation test across the NOAA, v2, and HadISST data for a period of 32 yr, varying from 1982 to 2016, over the complete TIO region. A correlation of more than 0.9 was observed (results not shown here) across

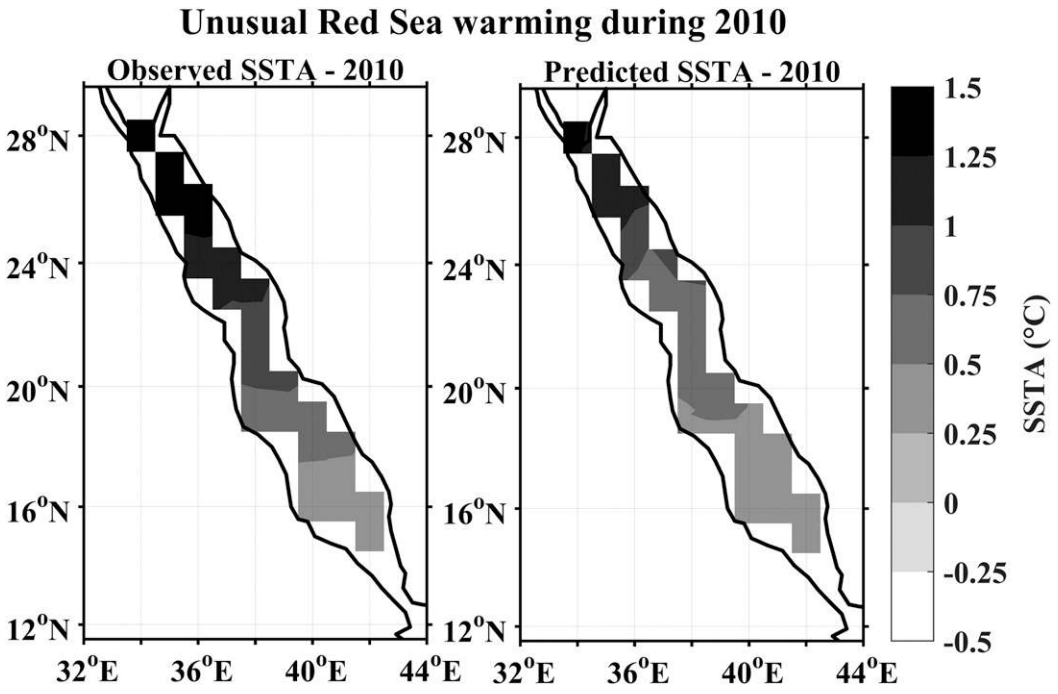

FIG. 10. Spatial variation of (left) observed SSTA vs (right) predicted SSTA during the warmest year, 2010, over the Red Sea. Note: Both observed and predicted SSTA were averaged over all months in the year 2010.

these datasets in almost every part of the TIO except for a small region in the EIO. This indicated an appropriateness of the NOAA data in the gap filling of the HadISST data.

Trained ANN models for the WIO and EIO regions were fed with the abovementioned data, and predictions of SSTA were made for five time steps (months). Such predicted WIO and EIO SSTA indices were subtracted to get real-time IOD forecasts. Figure 11 shows an IOD forecast for a prediction horizon of 5 months, varying from November 2017 to March 2018. As the HadISST data were available until August 2017, the latest NOAA data for September and October 2017 have been used for in filling. We also compared our real-time ANN predictions with the IOD forecasts issued by the Bureau of Meteorology using POAMA. POAMA is a coupled model and has the Bureau of Meteorology Research Centre atmospheric model, version 3.0 (BMRC), as atmospheric component and Australian Community Ocean Model version 2.0 (ACOM2) as the ocean component. Figure 12 shows the POAMA's real-time forecast from November 2017 to July 2018 and indicates that the ANN predictions are comparable with the POAMA-based real-time forecast.

7. Discussion and conclusions

In this study we developed ANN-based models to predict monthly SSTA over a large spatial domain rather than at specific sites as in earlier studies with ANNs. The prediction horizon was of 9 months. The database used for this purpose was the HadISST reanalysis data available for more than 140 yr from January 1870 onward. The performance of such models was evaluated over the entire TIO region. The prediction skill for the lead time of one month was found to be very attractive with the correlation coefficient r exceeding 0.8 for most of the TIO region. Although the accuracy decreased for the higher 2 and 3 months lead time, still the r value was more than 0.6 for the eastern AS, BoB, and WIO regions and for the southern (12°–24°S) TIO region. It was found that the prediction skill of the developed ANNs was in general good over a lead time of 4 months. The ANN models performed well over the WIO and EIO regions up to 5 months and 4 months, respectively, as judged by the error statistics of r and NRMSE. Such ANN prediction skills were seen to be better than some physics-based and coupled models applied over the TIO region. The relative underperformance of the latter models could be due to the absence of any appropriate data assimilation scheme used in corresponding predictions. The correlation skills of ANN predictions were comparable with those of the CFSv2 coupled model. The seasonal predictive skills of ANNs were found to be more attractive in the WIO region than the same in the EIO region. The EIO region exhibited a less persistent SSTA time history and also showed rapid changes during the monsoon season

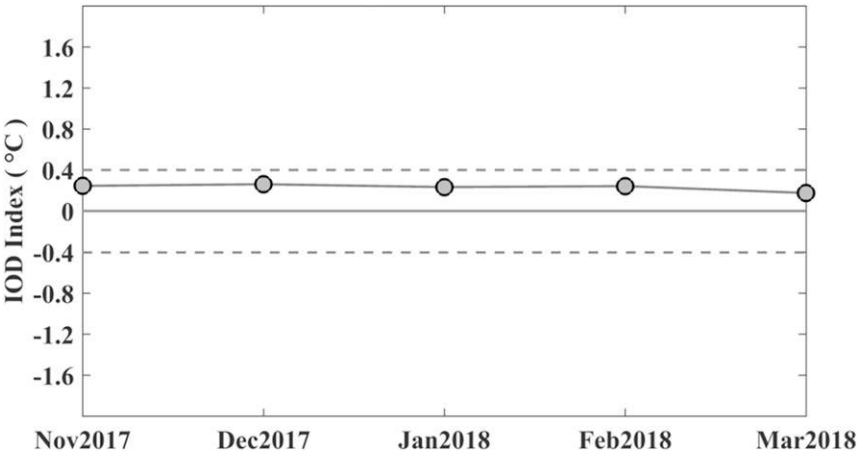

FIG. 11. Forecasts of the IOD index in real time using ANN models developed with HadISST data for November 2017 to March 2018. The horizontal lines indicate the limits for positive and negative IOD index. If the given index is beyond the horizontal dashed lines, then it is only recognized as a positive/negative IOD index.

leading to its underperformance in the EIO region. The skill of ANNs to predict the IOD events was better in the spring season than in late autumn; the skill of IOD predictions during the autumn season was affected as result of the moderate skill of SSTA prediction in the EIO region for autumn. This suggests that the IOD prediction skill was mainly controlled by the SSTA prediction skill in the EIO region during autumn.

The ANN predictions had shown good response in capturing prominent oceanic events. Both pIOD and nIOD were simulated satisfactorily. The less strong event of 1994 pIOD was more prominently captured than the 1997 pIOD event.

Similar results were seen for the basin-scale prediction of the IOD events in which the warming in the year 2000 was well predicted than the more severe warming of 2008. Further, the 1996 nIOD was better predicted than both pIOD events. Abrupt warming of the Red Sea was also reflected reasonably in the ANN predictions. In some regions a bias (cold or warm) was observed in the ANN-predicted SSTA, which could be due to high data nonlinearity for a given ANN architecture to model.

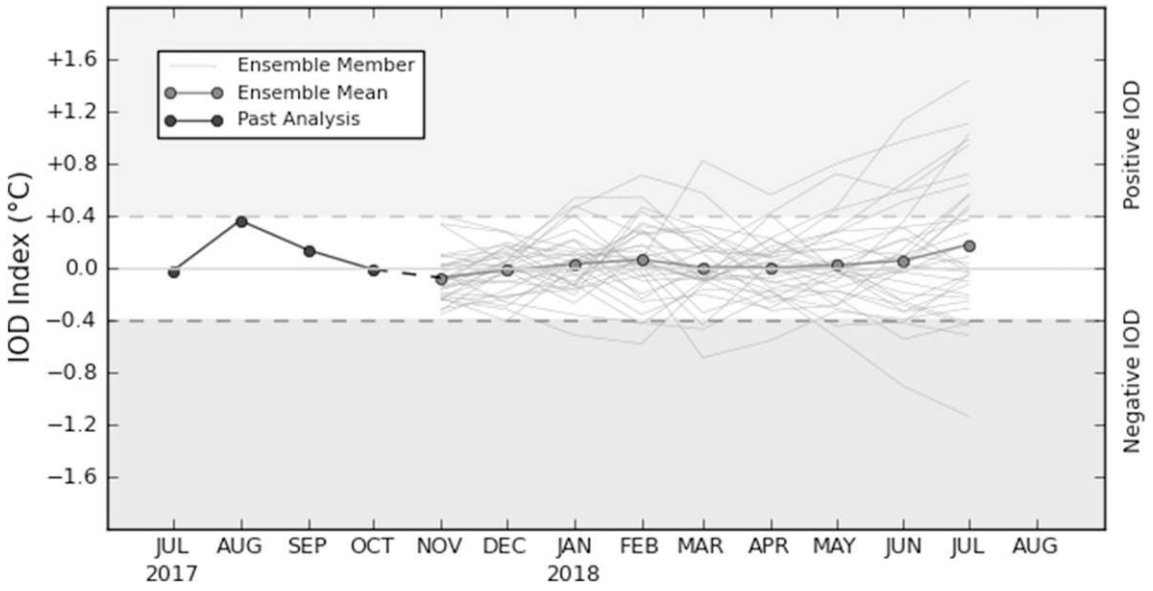

FIG. 12. Real-time IOD forecasts by the POAMA coupled model. IOD forecasts from 30 different ensembles (gray thin lines) and ensemble mean IOD forecasts (gray thick line for ensemble mean and black for past analyses; adapted from Australian Bureau of Meteorology 2017).

However, such bias was also seen in earlier coupled models (Huang et al. 2007; Xue et al. 2013; Zhu et al. 2015). In the future, bias removal schemes can be adopted to address this issue. Similarly, the use of alternative networks can also help in improving the network performance (Patil et al. 2016; Patil and Deo 2017).

It is reported that extreme IOD events might happen more frequently in the future (Cai et al. 2014). The pIOD and nIOD events can cause increasing floods and droughts, respectively, in India as well as in the countries surrounding the TIO. The pIOD and nIOD are, respectively, associated with the rise and fall of tropical cyclone frequency. Singh (2008) reported that such a heightened frequency of the tropical cyclones in the postmonsoon season had a lag of 2 months with the nIOD. Thus, the IOD prediction discussed in this work can help not only in forewarning flood or droughts but also the tropical cyclones in the countries surround the TIO region. Similarly, the prediction of the IOD along with that of unusual basin warming can help in issuing an advisory for fish landing patterns (Lan et al. 2013), bleaching of coral reefs, and wildfires (Abram et al. 2003).

In the exercise of real-time prediction of IOD events during the five months of November 2017–March 2018, it was found that the ANN predictions were comparable to IOD predictions from POAMA. However, there was a slight decreasing trend in the predicted real-time IOD that was contrary to POAMA. This inconsistency may have arisen from adding the latest data from NOAA, v2, to the HadISST data.

In summary we can say that ANN is an attractive and workable alternative to complex physics-based coupled models that additionally require a large amount of tuning effort. The ANN-based models can be postprocessed with appropriate bias correction procedures to enhance their performance (Chen et al. 2000; Chisanga et al. 2017).

Acknowledgments. We would like to express our sincere gratitude to Dr. Rayner and team from the Met Office Hadley Centre, who are associated with the HadISST reanalysis data. We would also express our sincere thanks to Dr. Reynolds and team from the NOAA ESRL PSD for the NOAA, v2, near-real-time SST dataset.

APPENDIX

Input Combinations for Modeling Monthly SSTA

Various combinations of preceding values in a given SSTA time series were selected as input to the ANNs. Table A1 shows some examples.

TABLE A1. Example of the input combinations for modeling monthly SSTA.

Input cases	Input combinations with past and seasonal values
1	1 2 3 4
2	1 2 3 4 6 12 18 24 30 36
3	1 2 3 4 12
4	1 2 3 4 12 24 36 48 60 72
5	1 2 3 4 6 12 24
6	1 2 3 4 6 12 18 24 30 36 48 60 72
7	1 2 3 4 5 6 7 8 9 10 11 12 13 14 15 16 17 18 24 36
8	1 2 3 4 5 6 7 8 9 10 11 12 13 14 15 16 17 18 24 30 36 42 48 54 60 72 84

REFERENCES

Abram, N. J., M. K. Gagan, M. T. McCulloch, J. Chappell, and W. S. Hantoro, 2003: Coral reef death during the 1997 Indian Ocean dipole linked to Indonesian wildfires. *Science*, **301**, 952–955, https://doi.org/10.1126/science.1083841.

Agarwal, N., C. M. Kishtawal, and P. K. Pal, 2001: An analogue prediction method for global sea surface temperature. *Curr. Sci.*, **80**, 49–55.

Aguilar-Martinez, S., and W. W. Hsieh, 2009: Forecasts of tropical Pacific sea surface temperatures by neural networks and support vector regression. *Int. J. Oceanogr.*, **2009**, 167239, https://doi.org/10.1155/2009/167239.

Álvarez, A., 2003: Performance of satellite-based ocean forecasting (SOFT) systems: A study in the Adriatic Sea. *J. Atmos. Oceanic Technol.*, **20**, 717–729, https://doi.org/10.1175/1520-0426(2003)20<717:POSBOF>2.0.CO;2.

——, Orfila, A., and Tintoré, J, 2004: Real-time forecasting at weekly timescales of the SST and SLA of the Ligurian Sea with a satellite-based ocean forecasting (SOFT) system. *J. Geophys. Res.*, **109**, C03023, https://doi.org/10.1029/2003JC001929.

Alves, O., and Coauthors, 2003 POAMA: Bureau of Meteorology operational coupled model seasonal forecast system. *Science for Drought: Proceedings of the National Drought Forum*, R. Stone and I. Partridge, Eds., State of Queensland Department of Primary Industries, 49–56.

Anderson, J. A., 1995: *An Introduction to Neural Networks.* MIT Press, 672 pp.

Australian Bureau of Meteorology, 2017: POAMA long-range outlook. Australian Bureau of Meteorology, accessed 5 November 2017, http://www.bom.gov.au/climate/poama2.4/poama.shtml.

Cai, W., and Coauthors, 2014: Increased frequency of extreme Indian Ocean Dipole events due to greenhouse warming. *Nature*, **510**, 254–258, https://doi.org/10.1038/nature13327.

Cantin, N. E., A. L. Cohen, K. B. Karnauskas, A. M. Tarrant, and D. C. McCorkle, 2010: Ocean warming slows coral growth in the central Red Sea. *Science*, **329**, 322–325, https://doi.org/10.1126/science.1190182.

Chen, D., M. A. Cane, S. E. Zebiak, R. Canizares, and A. Kaplan, 2000: Bias correction of an ocean-atmosphere coupled model. *Geophys. Res. Lett.*, **27**, 2585–2588, https://doi.org/10.1029/1999GL011078.

Cheng, L., K. E. Trenberth, J. Fasullo, T. Boyer, J. Abraham, and J. Zhu, 2017: Improved estimates of ocean heat content from

1960 to 2015. *Sci. Adv.*, **3**, e1601545, https://doi.org/10.1126/sciadv.1601545.

Chisanga, C. B., E. Phiri, and V. R. Chinene, 2017: Statistical bias correction of Fifth Coupled Model Intercomparison Project data from the CGIAR Research Program on Climate Change, Agriculture and Food Security-Climate Portal for Mount Makulu, Zambia. *Br. J. Appl. Sci. Technol.*, **21** (4), https://doi.org/10.9734/BJAST/2017/33531.

Choi, K. S., S. Park, K. H. Chang, and J. H. Lee, 2015: A possible relationship between East Indian Ocean SST and tropical cyclone affecting Korea. *Nat. Hazards*, **76**, 283–301, https://doi.org/10.1007/s11069-014-1489-5.

Collins, D. C., C. J. C. Reason, and F. Tangang, 2004: Predictability of Indian Ocean sea surface temperature using canonical correlation analysis. *Climate Dyn.*, **22**, 481–497, https://doi.org/10.1007/s00382-004-0390-4.

Deo, M. C., 2010: Artificial neural networks in coastal and ocean engineering. *Indian J. Geo-Mar. Sci.*, **39**, 589–596.

Emanuel, K. A., 2005: Increasing destructiveness of tropical cyclones over the past 30 years. *Nature*, **436**, 686–688, https://doi.org/10.1038/nature03906.

England, M. H., C. C. Ummenhofer, and A. Sen Gupta, 2009: Effect of tropical and subtropical Indian Ocean dipoles in driving precipitation around Indian Ocean rim countries. *Extended Abstracts*, *A Changing Climate: Western Australia in Focus*, Crawley, Perth, WA, Australia, Western Australia Marine Science Institution, 15–16, https://www.wamsi.org.au/sites/wamsi.org.au/files/A%20Changing%20Climate%20abstract%20papers%20VF.pdf.

Francis, P. A., P. N. Vinayachandran, and S. S. C. Shenoi, 2013: The Indian Ocean forecast system. *Curr. Sci.*, **104**, 1354–1368.

Garcia-Gorriz, E., and J. Garcia-Sanchez, 2007: Prediction of sea surface temperatures in the western Mediterranean Sea by neural networks using satellite observations. *Geophys. Res. Lett.*, **34**, L11603, https://doi.org/10.1029/2007GL029888.

Guan, Z., and T. Yamagata, 2003: The unusual summer of 1994 in East Asia: IOD teleconnections. *Geophys. Res. Lett.*, **30**, 1544, https://doi.org/10.1029/2002GL016831.

Gupta, S. M., and B. A. Malmgren, 2009: Comparison of the accuracy of SST estimates by artificial neural networks (ANN) and other quantitative methods using radiolarian data from the Antarctic and Pacific Oceans. *Earth Sci. India*, **2**, 52–75.

Hagan, M. T., and M. B. Menhaj, 1994: Training feedforward networks with the Marquardt algorithm. *IEEE Trans. Neural Networks*, **5**, 989–993, https://doi.org/10.1109/72.329697.

Huang, B., Z. Z. Hu, and B. Jha, 2007: Evolution of model systematic errors in the tropical Atlantic basin from coupled climate hindcasts. *Climate Dyn.*, **28**, 661–682, https://doi.org/10.1007/s00382-006-0223-8.

Jain, P., and M. C. Deo, 2006: Neural networks in ocean engineering. *Ships Offshore Struct.*, **1**, 25–35, https://doi.org/10.1533/saos.2004.0005.

Jansen, M. F., D. Dommenget, and N. Keenlyside, 2009: Tropical atmosphere–ocean interactions in a conceptual framework. *J. Climate*, **22**, 550–567, https://doi.org/10.1175/2008JCLI2243.1.

Kawamura, R., M. Sugi, T. Kayahara, and N. Sato, 1998: Recent extraordinary cool and hot summers in East Asia simulated by an ensemble climate experiment. *J. Meteor. Soc. Japan*, **76**, 597–617, https://doi.org/10.2151/jmsj1965.76.4_597.

Krishnan, R., M. Mujumdar, V. Vaidya, K. V. Ramesh, and V. Satyan, 2003: The abnormal Indian summer monsoon of 2000. *J. Climate*, **16**, 1177–1194, https://doi.org/10.1175/1520-0442(2003)16<1177:TAISMO>2.0.CO;2.

Kug, J., I. Kang, J. Lee, and J. Jhun, 2004: A statistical approach to Indian Ocean Sea surface temperature prediction using a dynamical ENSO prediction. *Geophys. Res. Lett.*, **31**, L09212, https://doi.org/10.1029/2003GL019209.

Lan, K. W., K. Evans, and M. A. Lee, 2013: Effects of climate variability on the distribution and fishing conditions of yellowfin tuna (*Thunnusalbacares*) in the western Indian Ocean. *Climatic Change*, **119**, 63–77, https://doi.org/10.1007/s10584-012-0637-8.

Lee, P. F., I. C. Chen, and W. N. Tzeng, 2005: Spatial and temporal distribution patterns of bigeye tuna (*Thunnusobesus*) in the Indian Ocean. *Zool. Stud.*, **44**, 260–270.

Luo, J. J., S. Masson, S. Behera, S. Shingu, and T. Yamagata, 2005: Seasonal climate predictability in a coupled OAGCM using a different approach for ensemble forecasts. *J. Climate*, **18**, 4474–4497, https://doi.org/10.1175/JCLI3526.1.

Magee, A. D., D. C. Verdon-Kidd, and A. S. Kiem, 2015: Can Indian Ocean SST variability impact TC activity in the South Pacific? A spatial analysis. *Geophysical Research Abstracts*, Vol. 17, Abstract EGU2015-3126-1, https://meetingorganizer.copernicus.org/EGU2015/EGU2015-3126-1.pdf.

Mahongo, S. B., and M. C. Deo, 2013: Using artificial neural networks to forecast monthly and seasonal sea surface temperature anomalies in the western Indian Ocean. *Int. J. Ocean Climate Syst.*, **4**, 133–150, https://doi.org/10.1260/1759-3131.4.2.133.

Marquardt, D. W., 1963: An algorithm for least-squares estimation of nonlinear parameters. *J. SIAM*, **11**, 431–441, https://doi.org/10.1137/0111030.

Michaels, P. J., P. C. Knappenberger, and R. E. Davis, 2006: Sea-surface temperatures and tropical cyclones in the Atlantic basin. *Geophys. Res. Lett.*, **33**, L09708, https://doi.org/10.1029/2006GL025757.

Neetu, R. Sharma, S. Basu, A. Sarkar, and P. K. Pal, 2011: Data-adaptive prediction of sea-surface temperature in the Arabian Sea. *IEEE Geosci. Remote Sens. Lett.*, **8**, 9–13, https://doi.org/10.1109/LGRS.2010.2050674.

Patil, K., and M. C. Deo, 2017: Prediction of daily sea surface temperature using efficient neural networks. *Ocean Dyn.*, **67**, 357–368, https://doi.org/10.1007/s10236-017-1032-9.

——, ——, and M. Ravichandran, 2016: Prediction of sea surface temperature by combining numerical and neural techniques. *J. Atmos. Oceanic Technol.*, **33**, 1715–1726, https://doi.org/10.1175/JTECH-D-15-0213.1.

Raitsos, D. E., I. Hoteit, P. K. Prihartato, T. Chronis, G. Triantafyllou, and Y. Abualnaja, 2011: Abrupt warming of the Red Sea. *Geophys. Res. Lett.*, **38**, L14601, https://doi.org/10.1029/2011GL047984.

Rao, S. A., H. S. Chaudhari, S. Pokhrel, and B. N. Goswami, 2010: Unusual central Indian drought of summer monsoon 2008: Role of southern tropical Indian Ocean warming. *J. Climate*, **23**, 5163–5174, https://doi.org/10.1175/2010JCLI3257.1.

——, A. R. Dhakate, S. K. Saha, S. Mahapatra, H. S. Chaudhari, S. Pokhrel, and S. K. Sahu, 2012: Why is Indian Ocean warming consistently? *Climatic Change*, **110**, 709–719, https://doi.org/10.1007/s10584-011-0121-x.

Rayner, N. A., D. E. Parker, E. B. Horton, C. K. Folland, L. V. Alexander, D. P. Rowell, and A. Kaplan, 2003: Global analyses of sea surface temperature, sea ice, and night marine air temperature since the late nineteenth century. *J. Geophys. Res.*, **108**, 4407, https://doi.org/10.1029/2002JD002670.

Reddy, P. R. C., and P. S. Salvekar, 2003: Equatorial East Indian Ocean sea surface temperature: A new predictor for seasonal and annual rainfall. *Curr. Sci.*, **85**, 1600–1604.

Roxy, M. K., K. Ritika, P. Terray, and S. Masson, 2014: The curious case of Indian Ocean warming. *J. Climate*, **27**, 8501–8509, https://doi.org/10.1175/JCLI-D-14-00471.1.

Saha, K. K., and S. A. Wasimi, 2013: Interrelationship between Indian Ocean Dipole (IOD) and Australian tropical cyclones. *Int. J. Environ. Sci. Dev.*, **4**, 647–651, https://doi.org/10.7763/IJESD.2013.V4.431.

Saha, S., and Coauthors, 2006: The NCEP Climate Forecast System. *J. Climate*, **19**, 3483–3517, https://doi.org/10.1175/JCLI3812.1.

——, and Coauthors, 2014: The NCEP Climate Forecast System version 2. *J. Climate*, **27**, 2185–2208, https://doi.org/10.1175/JCLI-D-12-00823.1.

Sahai, A. K., A. M. Grimm, V. Satyan, and G. B. Pant, 2003: Long-lead prediction of Indian summer monsoon rainfall from global SST evolution. *Climate Dyn.*, **20**, 855–863, https://doi.org/10.1007/s00382-003-0306-8.

Saji, N. H., and T. Yamagata, 2003: Possible impacts of Indian Ocean dipole mode events on global climate. *Climate Res.*, **25**, 151–169, https://doi.org/10.3354/cr025151.

——, B. N. Goswami, P. N. Vinayachandran, and T. Yamagata, 1999: A dipole mode in the tropical Indian Ocean. *Nature*, **401**, 360–363, https://doi.org/10.1038/43854.

Sebastian, M., and M. R. Behera, 2015: Impact of SST on tropical cyclones in North Indian Ocean. *Procedia Eng.*, **116**, 1072–1077, https://doi.org/10.1016/j.proeng.2015.08.346.

Shi, L., H. H. Hendon, O. Alves, J. J. Luo, M. Balmaseda, and D. Anderson, 2012: How predictable is the Indian Ocean dipole? *Mon. Wea. Rev.*, **140**, 3867–3884, https://doi.org/10.1175/MWR-D-12-00001.1.

Shukla, J., and B. M. Misra, 1977: Relationships between sea surface temperature and wind speed over the central Arabian Sea, and monsoon rainfall over India. *Mon. Wea. Rev.*, **105**, 998–1002, https://doi.org/10.1175/1520-0493(1977)105<0998:RBSSTA>2.0.CO;2.

Singh, O. P., 2008: Indian Ocean dipole mode and tropical cyclone frequency. *Curr. Sci.*, **94**, 29–31.

Solanki, H. U., D. Bhatpuria, and P. Chauhan, 2015: Signature analysis of satellite derived SSHa, SST and chlorophyll concentration and their linkage with marine fishery resources. *J. Mar. Syst.*, **150**, 12–21, https://doi.org/10.1016/j.jmarsys.2015.05.004.

Stockdale, T. N., and Coauthors, 2011: ECMWF seasonal forecast system 3 and its prediction of sea surface temperature. *Climate Dyn.*, **37**, 455–471, https://doi.org/10.1007/s00382-010-0947-3.

Tang, B., W. W. Hsieh, A. H. Monahan, and F. T. Tangang, 2000: Skill comparisons between neural networks and canonical correlation analysis in predicting the equatorial Pacific sea surface temperatures. *J. Climate*, **13**, 287–293, https://doi.org/10.1175/1520-0442(2000)013<0287:SCBNNA>2.0.CO;2.

Thompson, B., C. Gnanaseelan, and P. S. Salvekar, 2005: Indian Ocean dipole simulation using Modular Ocean Model. Indian Institute of Tropical Meteorology Research Rep. RR-108, 35 pp.

Tripathi, K. C., M. L. Das, and A. K. Sahai, 2006: Predictability of sea surface temperature anomalies in the Indian Ocean using artificial neural networks. *Indian J. Geo-Mar. Sci.*, **35**, 210–220.

Ummenhofer, C. C., A. Sen Gupta, M. H. England, and C. J. Reason, 2009: Contributions of Indian Ocean sea surface temperatures to enhanced East African rainfall. *J. Climate*, **22**, 993–1013, https://doi.org/10.1175/2008JCLI2493.1.

Wang, G., and Coauthors, 2011: POAMA-2 SST skill assessment and beyond. CAWCR Research Letters 6, P. A. Sandery et al., Eds., Centre for Australian Weather and Climate Research, 40–46.

Wang, L., R. Huang, and R. Wu, 2013: Interdecadal variability in tropical cyclone frequency over the South China Sea and its association with the Indian Ocean sea surface temperature. *Geophys. Res. Lett.*, **40**, 768–771, https://doi.org/10.1002/grl.50171.

Webster, P. J., A. M. Moore, J. P. Loschnigg, and R. R. Leben, 1999: Coupled ocean–atmosphere dynamics in the Indian Ocean during 1997–98. *Nature*, **401**, 356, https://doi.org/10.1038/43848.

Wu, A., W. W. Hsieh, and B. Tang, 2006: Neural network forecasts of the tropical Pacific sea surface temperatures. *Neural Network*, **19**, 145–154, https://doi.org/10.1016/j.neunet.2006.01.004.

Xue, Y., and A. Leetmaa, 2000: Forecasts of tropical Pacific SST and sea level using a Markov model. *Geophys. Res. Lett.*, **27**, 2701–2704, https://doi.org/10.1029/1999GL011107.

——, M. Chen, A. Kumar, Z. Z. Hu, and W. Wang, 2013: Prediction skill and bias of tropical Pacific sea surface temperatures in the NCEP Climate Forecast System version 2. *J. Climate*, **26**, 5358–5378, https://doi.org/10.1175/JCLI-D-12-00600.1.

Yamagata, T., S. K. Behera, J.-J. Luo, S. Masson, M. R. Jury, and S. A. Rao, 2004: Coupled ocean-atmosphere variability in the tropical Indian Ocean. *Earth's Climate: The Ocean-Atmosphere Interaction*, *Geophys. Monogr.*, Vol. 147, Amer. Geophys. Union, 189–211, https://doi.org/10.1029/147GM12.

Yang, S., and K. M. Lau, 1998: Influences of sea surface temperature and ground wetness on Asian summer monsoon. *J. Climate*, **11**, 3230–3246, https://doi.org/10.1175/1520-0442(1998)011<3230:IOSSTA>2.0.CO;2.

Yasunaka, S., and K. Hanawa, 2011: Intercomparison of historical sea surface temperature datasets. *Int. J. Climatol.*, **31**, 1056–1073, https://doi.org/10.1002/joc.2104.

Yu, L., and M. J. McPhaden, 2011: Ocean preconditioning of Cyclone Nargis in the Bay of Bengal: Interaction between Rossby waves, surface fresh waters, and sea surface temperatures. *J. Phys. Oceanogr.*, **41**, 1741–1755, https://doi.org/10.1175/2011JPO4437.1.

Zhan, R., Y. Wang, and L. Tao, 2014: Intensified impact of East Indian Ocean SST anomaly on tropical cyclone genesis frequency over the western North Pacific. *J. Climate*, **27**, 8724–8739, https://doi.org/10.1175/JCLI-D-14-00119.1.

Zhu, J., B. Huang, A. Kumar, and J. L. Kinter III, 2015: Seasonality in prediction skill and predictable pattern of Tropical Indian Ocean SST. *J. Climate*, **28**, 7962–7984, https://doi.org/10.1175/JCLI-D-15-0067.1.